The Effect of Porosity on Fatigue of Die Cast AM60

CrossMark

ZHUOFEI YANG, JIDONG KANG, and DAVID S. WILKINSON

AM60 high-pressure die castings are known to contain significant porosity which can affect fatigue life. We have studied this using samples drawn from prototype AM60 shock towers by conducting strain-controlled fatigue tests accompanied by X-ray computed tomography analysis. The results show that the machined surface is the preferential location for fatigue crack development, with pores close to these surfaces serving as initiation sites. Fatigue life shows a strong inverse correlation with the size of the fatigue-crack-initiating pore. Pore shape and pore orientation also influence the response. A supplemental study on surface roughness shows that porosity is the dominant factor in fatigue. Tomography enables the link between porosity and fatigue crack initiation to be clearly identified. These data are complemented by SEM observations of the fracture surfaces which are generally flat and full of randomly oriented serration patterns but without long-range fatigue striations.

I. INTRODUCTION

MAGNESIUM'S low density and good castability makes it attractive to the automotive industry for improving fuel economy. Most of the magnesium alloy components in vehicles currently are fabricated from alloys such as AM60, using a high-pressure die casting (HPDC) process which is both cost effective and capable of producing a large volume of components with net shape and complex geometries.[1] However, the inherent porosity present in cast components impairs the mechanical performance, especially fatigue properties, and thus impedes the wider use of this material. There is therefore a need to better understand the effect of porosity on fatigue properties and reliability.

Several studies[2–6] have been conducted to characterize the effect of porosity on fatigue in cast alloys and some qualitative conclusions have been drawn. Most studies rely on fractographic analysis to assess, post-mortem, the pores that contribute to fatigue failure of the casting. Mohd et al.[2] have shown that the scatter in fatigue life is similar in AM60B and A356 castings but considerably less for rolled AM60B, as a result of the reduction in porosity following rolling. Two studies have shown that pores connected to the surface are more detrimental than internal pores.[4,6] It is also known that larger pores produce stronger stress concentration effects.[6] However, these studies have been limited by the complex three-dimensional nature of casting porosity which represents a challenge for characterization techniques that are typically two-dimensional, involving metallography and fracture surface analysis.

X-ray computed tomography (XCT), which offers a three-dimensional non-destructive characterization tool, has been utilized in several recent studies of fatigue.[7–10] XCT can provide a 3D assessment of the number, size, shape, and orientation of casting pores. We have recently demonstrated how XCT, coupled with more classical methods involving 2D metallography and SEM fractography, provides the most accurate assessment of casting porosity.[10,11] Applying these approaches to an AM60 prototype shock tower (see Figure 1), we were able to demonstrate how the gas and shrinkage pores that populate the casting differ in size, shape, and location within the component. Li et al.[9] have shown how XCT analysis can be linked to measurements of the fatigue response in an Al alloy, thus providing more reliable parameters for fatigue modeling and simulation.

This paper builds on a preliminary study of fatigue in AM60[10] in which we have shown that fatigue cracks are indeed nucleated at large pores and that XCT, coupled with interrupted testing, can track this initiation and the initial growth process. That work examined a few pores only. In this paper, we take a more quantitative approach based on a larger sample size and use XCT data to correlate the size and volume fraction of porosity in each sample with the measured fatigue life.

II. EXPERIMENTAL

All specimens tested in the present study were extracted from shock towers made via high-pressure die casting using the AM60 Mg alloy. The material was provided by CanmetMATERIALS. The chemical composition is given in Table I. Specimens were machined from 6 locations, as marked on the shock tower shown in Figure 1, and they all have the same thickness of 3 mm. Previous work shows that the overall porosity

ZHUOFEI YANG, Graduate Student, is with McMaster University, 1280 Main Street West, Hamilton, ON L8S 4L8 Canada, and also with CanmetMATERIALS, Natural Resources Canada, 183 Longwood Road South, Hamilton, ON L8P 0A5, Canada. JIDONG KANG, Research Scientist, is with CanmetMATERIALS, Natural Resources Canada. Contact e-mail: jidong.kang@canada.ca DAVID S. WILKINSON, Distinguished University Professor, is with McMaster University.
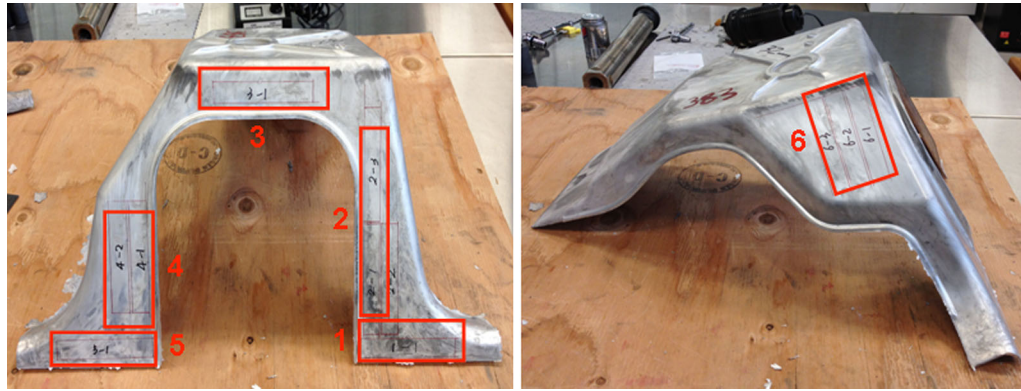
Fig. 1—Shock tower used in present study with 6 locations marked for specimen preparation.

Table I. Chemical Composition of AM60 Mg Alloy in Weight Percent

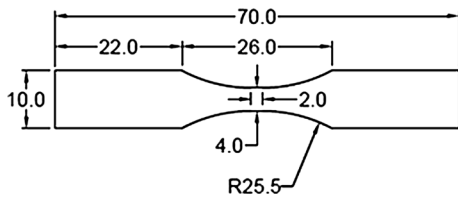| Mg	Al	Mn	Si	Zn	Sn	Pb	Fe	Cu	Ni	Be
Bal.	6.0	0.37	<0.01	<0.01	<0.01	<0.01	0.003	<0.001	<0.001	<0.001

Fig. 2—Specimen geometry used in present study, all dimensions are in mm.

levels and pores size distributions are similar at each location.[10]

Fatigue specimens with a flat dog bone shape, as shown in Figure 2, were prepared by electrical discharge machining (EDM). The original casting surface was preserved. The machined side surfaces in the cross-section-reduced region were manually ground with SiC papers to 600 grit. Grinding was performed only in the longitudinal direction to avoid transverse scratches, which would act as stress concentrators. Machining specimens from a fabricated part, in this case a casting, inevitably introduces a new surface condition. A number of specimens were further polished on the machined surfaces to compare both surface finish and its impact on fatigue. This was achieved by grinding with 1200 grit and then polishing with diamond suspensions down to 1 μm and finally polishing with a 0.05 μm colloidal silica suspension. An optical surface profiler was used to measure surface roughness for each surface condition present on a fatigue specimen: as-cast surface; EDM machined surface; machined and ground surface; and machined and polished surface.

Strain-controlled fatigue tests were conducted at six strain levels with the strain amplitude ranging from 0.2 to 0.8 pct. All tests were performed at room temperature with a strain ratio $R = -1$ and frequency 0.5 Hz. A 6-mm extensometer was attached to the specimen to measure the longitudinal strain. A fatigue test was stopped when the tensile load dropped below the stable value by 10 pct, which was defined as the point of failure. This prevented the fatigue damage on the fracture surface from being obliterated due to cyclical contacts during the final cycles.

X-ray tomography scan was performed using a Skyscan 1172 high-resolution micro-CT scanner. All specimens tested in fatigue were XCT scanned prior to and after testing. The initial scan revealed the internal porosity, enabling the measurement of parameters that are related to each pore such as volume, surface area, sphericity, and the centroid coordinates.[11] A final scan was conducted following fatigue testing to produce a 3D reconstruction of the fatigue cracks and associated pores. The observation of fatigue cracks and the associated pores in 3D also helps in locating the pores that initiated each fatigue crack in the initial XCT scan. This is expected to assist with and complement failure analysis by SEM observation. From a tomography perspective, cracks represent voids that are rather thin in one direction. This presents a challenge near the crack tip where the opening can be similar to or less than the pixel size. In this case, some of the crack will be missing in the tomographic image. This issue is exacerbated by the process of crack closure[12] that occurs when the specimen is unloaded, leading to a further underestimation in crack length. To overcome this, a tensile fixture was devised,[10] made from a plastic tube that applied a small tensile force to the specimen so that the crack surfaces remain open during the XCT scans. The plastic tube, because it absorbs very few X-rays in comparison with a metal, does not affect the XCT results. The X-ray source operates at a voltage of 60 kV for all XCT scans. The scan covers a region 6 mm long in the center of the specimen. The pixel size was set at 6.05 μm for the initial
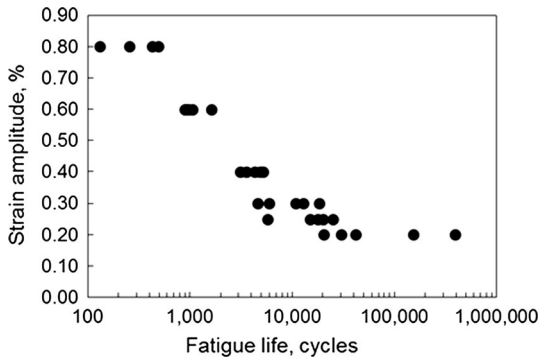
Fig. 3—Fatigue life as a function of strain amplitude.

Fig. 4—Surface roughness measurements in each surface condition (Color figure online).

scans as porosity is easier to be detected, and was resized to 3.02 μm for final scans to achieve a higher resolution to detect possible fatigue cracks. More details on this technique have been published elsewhere.[10]

The XCT scans of fatigue cracked specimens enable the visualization of fatigue cracks and the associated pores, from which the crack initiation sites could be determined by considering the fatigue crack shape. However, due to the limited resolution of this technique (which is a few microns), detailed microstructural features, such as fatigue striation patterns, will not be observed. Therefore, fracture surfaces were observed *via* SEM. As noted above, fatigue testing was stopped before fracture had occurred. Therefore, once XCT scanning was completed, samples were broken in uni-axial tension to reveal the fracture surface. SEM observations were used to study the fatigue cracked region at high resolution and to compare these observation with the XCT scans. Both fracture surfaces of a specimen were observed. The fracture surface observations were performed using a Philips XL 30 SEM at CanmetMATERIALS.

III. RESULTS AND DISCUSSION

A. *Fatigue Test Results*

Figure 3 shows the fatigue life *N* as a function of strain amplitude for fatigue tests at six strain amplitudes. At each strain level, 5 specimens with the same machined surface condition (ground to 600 grit) were tested; some specimens shared similar fatigue lives so the data points overlap. As seen from the figure, lower strain levels are subject to a larger scatter of fatigue life: the scatter of fatigue lives at a strain amplitude of 0.2 pct is more than one order of magnitude.

B. *The Effect of Surface Roughness on Fatigue Life*

Given that the specimen preparation introduces new surfaces and fatigue properties are sensitive to the surface condition, the effect of surface conditions on fatigue life was studied to distinguish it from the impact of pores on fatigue. Figure 4 shows the surface roughness measurements. Sa, expressing the average of the
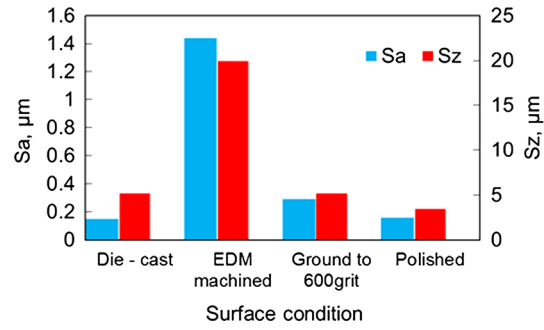
absolute values of the height in the measured area, is less affected by a single peak or valley and represents the overall surface condition. Sz, on the other hand, expressed as the average of 5 sets of the highest peaks plus the lowest valleys, measures the maximum height present in the measured area. Their formulas are given as

$$S_a = \frac{1}{A} \iint_A |Z(x,y)| \mathrm{d}x\mathrm{d}y$$

$$S_z = \frac{1}{5} \sum_{i=1}^{5} R_{pi} + R_{vi}$$

where *A* is the area of measured region, $R_{p\,i}$ and $R_{v\,i}$ correspond to the *i* th highest peak and the *i* th lowest valley, respectively.

Detailed observations of surfaces in different conditions are shown in Figure 5. The as-cast surface has quite a smooth surface finish while EDM machining results in a faceted machined surface with extremely high values of Sa and Sz. Manual grinding improves the surface condition considerably although it is still inferior to the cast surface, presenting parallel scratches on the surface (Figure 5(c)). Polishing produces a surface condition that is comparable to the cast surface.

At an even higher magnification, the microstructure on the machined and polished surface (Figure 6) reveals a height difference between the α-Mg phase (blue), the eutectic phase (green), and the dispersed particles (red). In Figure 6(b), a particle is measured to protrude more than a micron above an α-Mg grain. This explains why polishing does not improve the surface finish as compared to the as-cast surface. The height difference could result from the fact that particles are more resistant to polishing. It may be also because α-Mg is more susceptible to attack by colloidal silica, which works both mechanically and chemically on the specimen.

The fatigue lives of specimens tested in two surface conditions were compared. Six specimens with machined and ground surfaces were compared with five specimens that had machined and polished surfaces under the same test condition at a strain amplitude of 0.3 pct. The polished samples with a standard deviation of 3314 cycles showed a reduced scatter in the fatigue life,
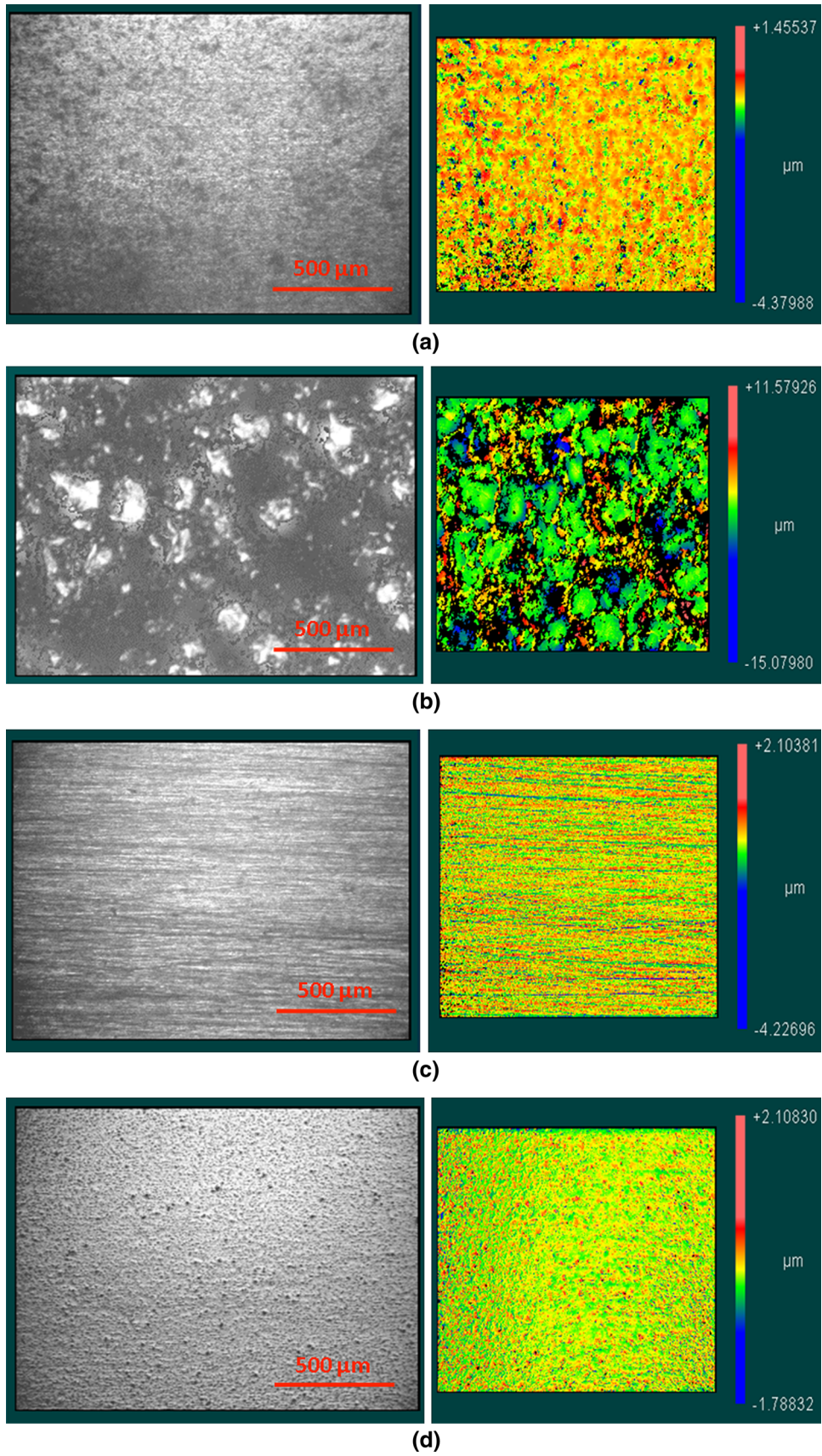
Fig. 5—Surface images and corresponding roughness plots for materials with different surface conditions: (*a*) die-cast surface; (*b*) EDM machined surface; (*c*) surface ground to 600 grit; and (*d*) polished surface (Color figure online).
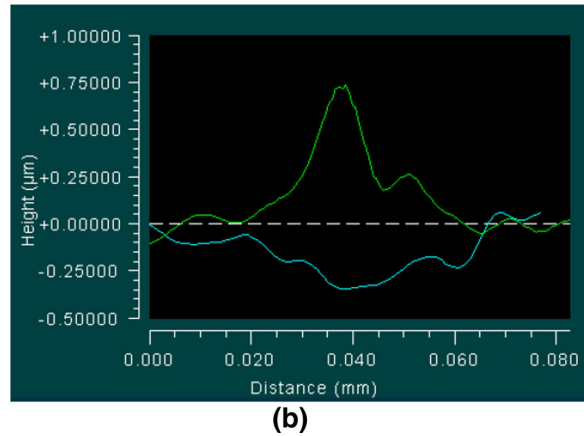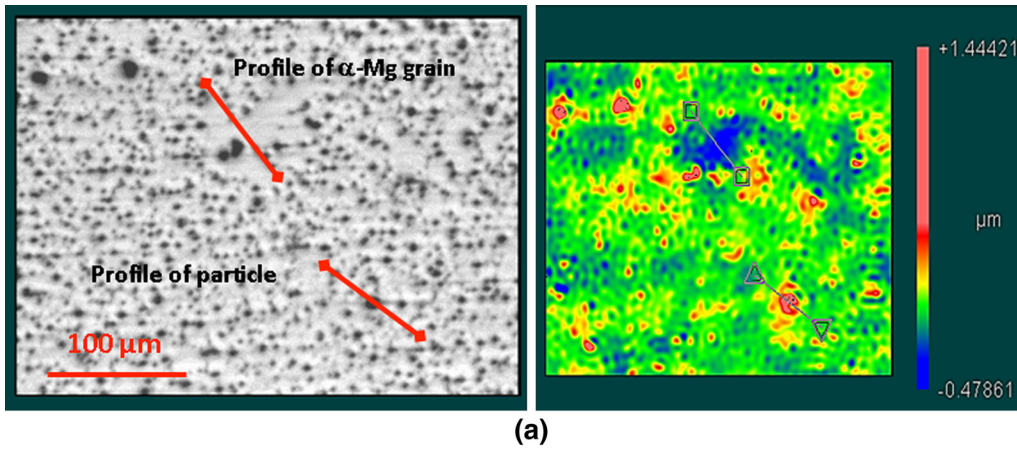
(a)

(b)

Fig. 6—Microstructure of a polished machined surface: (*a*) live display and surface contour plot; (*b*) two surface profiles: the green profile is drawn over a particle along the trajectory outlined in the lower right portion of the contour plot while the blue profile is drawn through the Mg phase along the trajectory outlined in the upper portion of the contour plot (Color figure online).
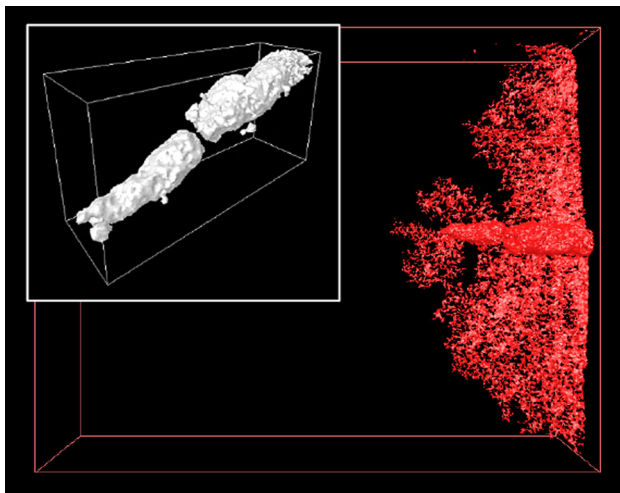

Fig. 7—3D reconstruction of fatigue cracks and the associated pores. The inset figure shows a detailed image of the casting pores serving as the crack initiation site, taken from the XCT scan performed prior to the start of the fatigue test.

compared with the standard deviation of ground samples being 5525 cycles. However, they did not exhibit a measurable improvement in average fatigue life, which is about 10,000 cycles in both cases.

C. *Fatigue Failure Analysis*

X-ray tomography scans, conducted on all failed specimens, revealed many cracks associated with casting pores, which had clearly served as the crack initiation sites. Most of the specimens were found to have fractured from a pore or a cluster of pores on, or just underneath, the machined surface. A few of the samples fractured from casting surface scratches, not associated with any particular pore. The machined surface is the preferred location for crack initiation for all specimens, including those in the machined and polished surface condition. This crack initiation site determination was later verified by SEM observations of the fracture surfaces.

Figure 7 shows a 3D reconstruction of the fatigue cracks in one specimen tested at a strain amplitude of 0.25 pct. The fatigue cracks are semi-elliptical in shape, centered on a pair of pores, which clearly served as the crack initiation site. These same pores were found in the XCT scan performed before testing, as shown in the inset on Figure 7. They are found adjacent to each other but positioned at slightly different height levels. The discontinuity of the fatigue crack around the pore further from the machined surface indicates that the crack that initiated from the pore on the machined surface was partially hindered from further propagation
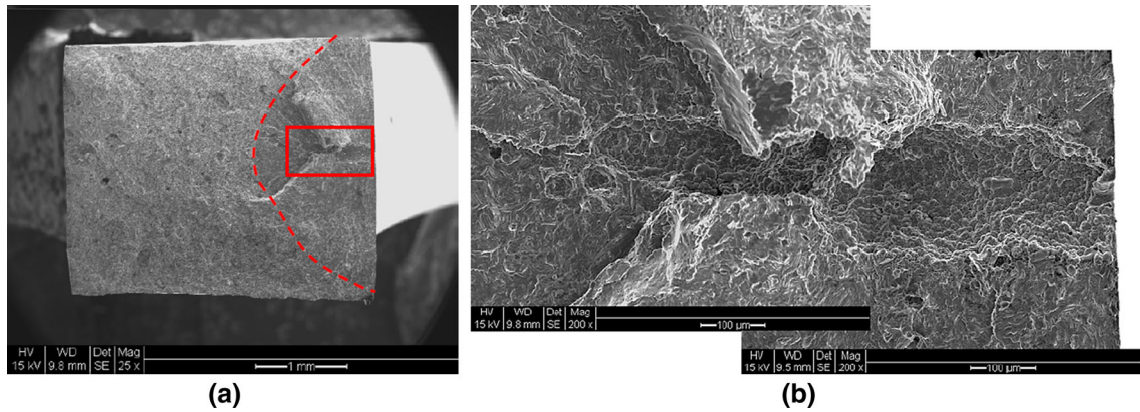
Fig. 8—(*a*) The overall fracture surface of the specimen of which the 3D reconstruction is shown in Fig. 7, and (*b*) the casting pores serving as crack initiation site.
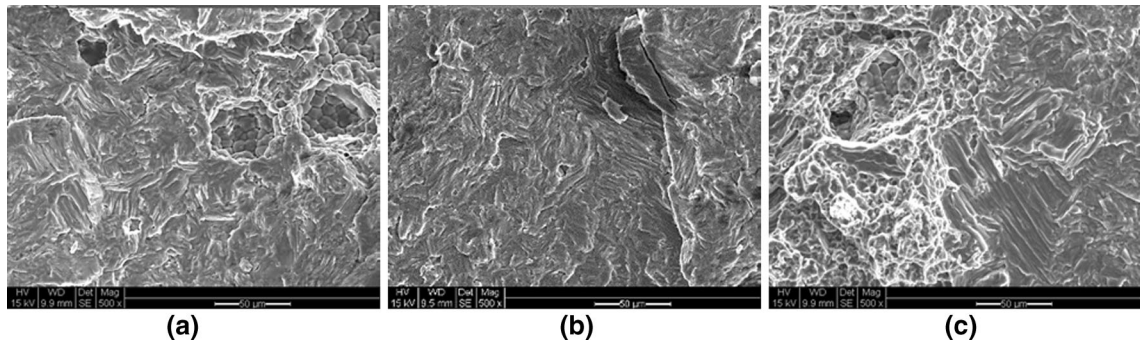

Fig. 9—The fracture surface in a region (*a*) near crack initiation site; (*b*) a distance from crack initiation site; (*c*) close to ductile fracture region.

when it met the pore further from the machined surface. A second fatigue crack was initiated from that pore which propagated at another height. No overlap of fatigue cracks was found. One possibility is that, once the growing fatigue crack encountered the second pore, a new crack was initiated there. The other is that the second crack had already nucleated and once they started to overlap their growth stopped. This makes sense since the opening of a fatigue crack relieves stress in the surrounding vicinity.

SEM observations of fracture surfaces were also performed. Figure 8 shows the fracture surface of the same specimen shown in Figure 7. The fatigued fracture surface is outlined in red to distinguish it from the final ductile fracture which occurred after the test when the specimen was pulled apart. The two levels on which the cracks propagated are clearly visible in this image. The two casting pores serving as the crack initiation site are shown at higher magnification in Figure 8(b). A pore on the fracture surface is easily recognized because of the appearance of intact dendrite cells on the surface.

Some of the microstructural features of the fatigue crack in three different regions (near the crack initiation site, away from the initiation site and close to the fatigue/ductile fracture transition region) are shown in Figure 9. Near the crack initiation site, the fracture surface is flat with randomly orientated serrations, indicating the local crack propagation directions.

Further from the crack initiation site, the fracture surface is also flat with fine serrations locally. The fracture surface in the fatigue/ductile region exhibits distinct microstructural features of each fracture mode. These observations suggest that fatigue crack propagation is stochastic throughout the fatigue process. Even in the later stages, fatigue crack growth does not become organized leading to large scale fatigue striations or beach marks. Only local effects of grain size dimensions are observed. This suggests that some grains fail by gradual fatigue crack propagation while others fail catastrophically when a critical condition is reached.

D. *The Impact of Individual Pore Features on Fatigue*

As noted above, some fatigue specimens did not fail from cracks initiated at pores. These have been removed from the data and the fatigue life data for the remaining samples are plotted in Figure 10. A linear relationship was found between strain amplitude and fatigue life when plotted on a log–log scale indicative of the power-law Coffin–Manson relationship for low cycle fatigue.

These data show considerable scatter. We speculate that it is due to the effect of the pore size that initiates each fatigue crack. The effect of strain amplitude on fatigue life is represented by the Coffin–Manson law. We can therefore multiply the strain amplitude by $N^{0.243}$ to
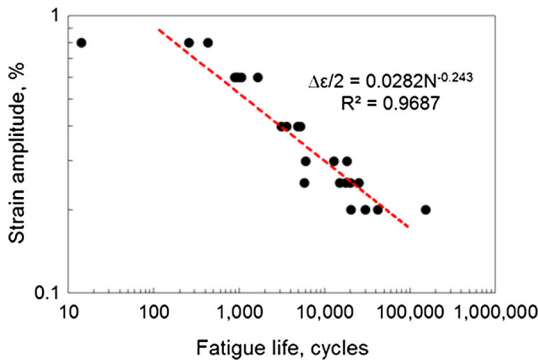
Fig. 10—Fatigue life curve with only those specimens fractured from porosity, fitted to the Coffin–Manson relationship.
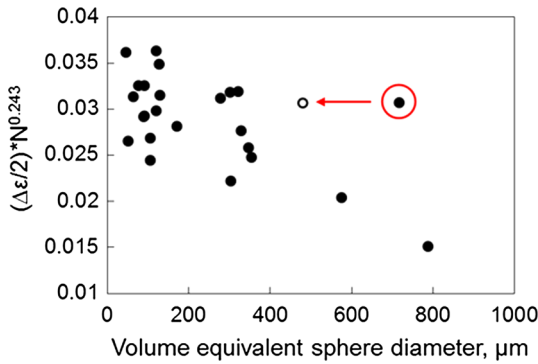

Fig. 11—Strain amplitude normalized by fatigue life, according to the Coffin–Manson relationship, plotted as a function of size of the pore serving as the crack initiation site. The circled data point exhibits the effect of pore shape and pore orientation, as outlined in the text.

produce a master curve which reveals the effect of porosity. Figure 11 shows the normalized fatigue life, as a function of the pore size at the crack initiation site for each failed sample. Here pore size is defined as the diameter of a spherical pore having the same volume as the 3D pore measured by XCT.

While large pores with a size of 400–800 μm are more damaging and can result in considerably shorter fatigue life, they are rare in the material such that most samples do not contain such pores in the gage section. Therefore, most specimens fail from pores smaller than 400 μm. Indeed, for most samples, the pore that initiates the fatigue failure is the largest pore that is on or reasonably close to the machined surface. For the purpose of comparison, we identify as "close-to-surface" pores those that are situated at a distance from the machined surface less than half of their size. This definition was used in Mayer's study[13] to separate surface porosity from internal porosity. The general trend suggests that at all strain levels, the fatigue life is decreased when the pore size serving as the crack initiation site becomes larger. A similar but less severe trend was shown in the study by Rettberg et al.[14] As pore size is measured differently in two studies, some difference in relationship can be expected. One data point, circled in the plot, is found to have deviated significantly from the general trend. This specimen is shown in Figure 12. This pore is elongated in the loading direction, such that the pore size measured on the fracture surface is much smaller than the diameter based on the volume. The pore size calculated by volume is 715 μm whereas as the average diameter of the pore measured on the fracture surface is only 479 μm. Using this revised value would shift this data point to the open circle in Figure 11. This pore represents a somewhat extreme case for the effect of
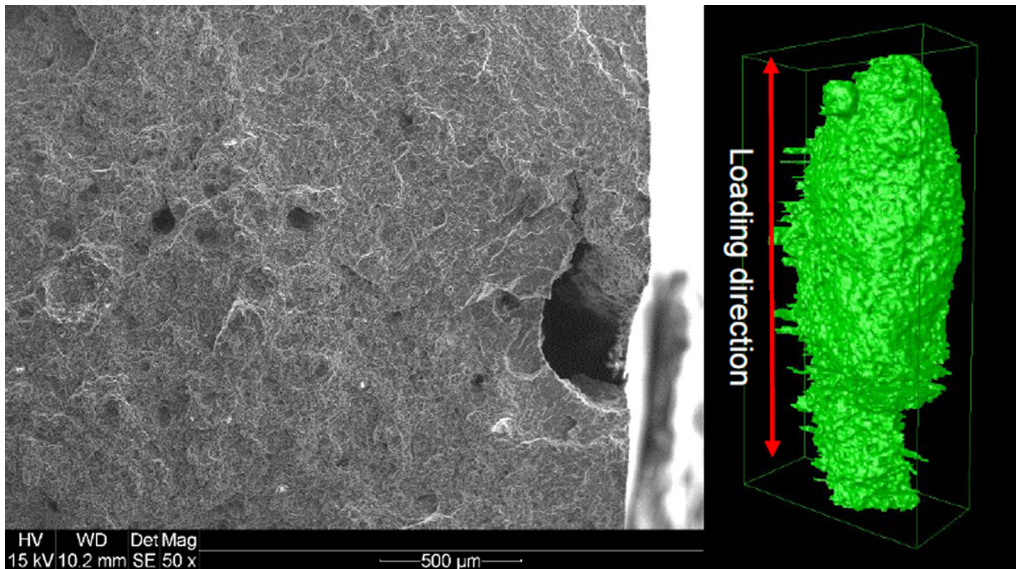

Fig. 12—SEM image showing a casting pore leading to the fatigue fracture and the corresponding 3D reconstruction of the pore prior to testing.
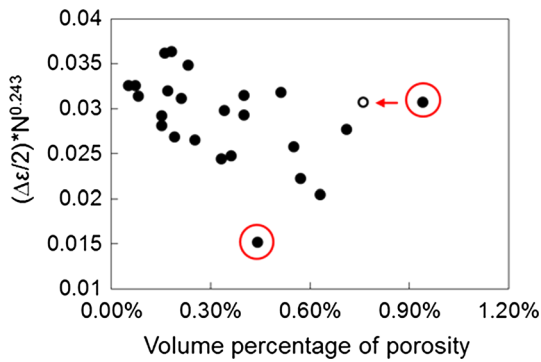
Fig. 13—A function of fatigue life and strain level *vs.* the volume fraction of porosity. The circled data point for a porosity of about 1 pct corresponds to the pore shown in Fig. 12. The other circled data point represents the effect of a single large pore which resulted in the local volume fraction of porosity around the pore higher than the global value.

pore orientation and pore shape on fatigue life. For the similar-sized pores, as shown in Figure 11, pore shape and pore location are secondary factors, that may account for some of the scatter in fatigue life. The study by Lu *et al.*[15] also concluded that the fatigue crack initiation process was sensitive to pore shape and loading direction (*i.e.*, pore orientation). Therefore, the orientation and shape of a pore are seen to be additional parameters which can influence fatigue life.

The volume fraction of porosity within the gage section was also measured by XCT. The normalized fatigue life is correlated with this parameter, as shown in Figure 13. This shows a similar downward trend. The two circled data points are observed to deviate from the general trend. The circled data point for a porosity of about 1 pct corresponds to the same pore shown in Figure 12, and once shape is taken into account as already discussed, the effect of porosity is decreased as shown. The other circled data point represents a specimen which failed from a surface pore with a diameter of 787 μm, this being the largest pore that served as the crack initiation site in the present study. Despite this large pore, this sample had overall a rather low porosity level.

While these plots suggest that both the size of fatigue crack initiating pore and the overall porosity influence fatigue life, this is in fact misleading. There is a relatively strong correlation between these parameters, *i.e.*, the largest pores are found in samples with the highest porosity. Based on our microstructural observations, it is really the size of the largest pores that control the fatigue life of the material. Porosity measurements, however, could possibly be used as a proxy for pore size.

IV. CONCLUSIONS

Samples extracted from prototype shock towers made from the AM60 Mg alloy *via* high-pressure die casting were fatigue tested. Strain-controlled fatigue tests were performed with specimens XCT scanned prior to and following testing, enabling the 3D characterization of porosity and fatigue cracks. The major findings are summarized as follows:

1. The machined surface is the preferred site for crack initiation. Nearly all specimens failed from fatigue cracks initiated at pores close to or on the machined surface.
2. By normalizing the fatigue life by the strain amplitude, it was possible to extract the dependence of fatigue life on porosity. The fatigue life decreases significantly as the size of the fatigue-crack-initiating pore increases. The same trend was also found between the volume fraction of porosity and the fatigue life.
3. Pore shape and pore orientation mostly likely represent secondary factors which also influence fatigue life.
4. Surface roughness was not found to have a major impact on the fatigue life.
5. The observations and measurements of porosity and fatigue cracks made by XCT were confirmed by SEM imaging of fracture surfaces, suggesting that XCT can be used as a reliable characterization tool for both porosity and fatigue crack propagation.
6. SEM observations showed that the fatigue fracture surfaces are generally flat with numerous randomly oriented serrations but no long-range fatigue striations.

REFERENCES

1. A.A. Luo: *J. Magnes. Alloy.*, 2013, vol. 1 (1), pp. 2–22.
2. S. Mohd, Y. Mutoh, Y. Otsuka, Y. Miyashita, T. Koike, and T. Suzuki: *Eng. Fail. Anal.*, 2012, vol. 22, pp. 64–72.
3. P. Mu, Y. Nadot, C. Nadot-Martin, A. Chabod, I. Serrano-Munoz, and C. Verdu: *Int. J. Fatigue*, 2014, vol. 63, pp. 97–109.
4. Y. Nadot, J. Mendez, N. Ranganathan, and A.S. Beranger: *Fatigue Fract. Eng. Mater. Struct.*, 1999, vol. 22 (4), pp. 289–300.
5. H.R. Ammar, A.M. Samuel, and F.H. Samuel: *Mater. Sci. Eng. A*, 2008, vol. 473 (1–2), pp. 65–75.
6. Y.X. Gao, J.Z. Yi, P.D. Lee, and T.C. Lindley: *Fatigue Fract. Eng. Mater. Struct.*, 2004, vol. 27 (7), pp. 559–70.
7. J.Y. Buffière, S. Savelli, P.H. Jouneau, E. Maire, and R. Fougères: *Mater. Sci. Eng. A*, 2001, vol. 316 (1–2), pp. 115–26.
8. G. Nicoletto, R. Konečná, and S. Fintova: *Int. J. Fatigue*, 2012, vol. 41, pp. 39–46.
9. P. Li, P.D. Lee, D.M. Maijer, and T.C. Lindley: *Acta Mater.*, 2009, vol. 57 (12), pp. 3539–48.
10. Z. Yang, J. Kang, and D.S. Wilkinson: *Metall. Mater. Trans. B*, 2015, vol. 46B, pp. 1576–85.
11. Z. Yang, A. Maurey, J. Kang, and D.S. Wilkinson: *Mater. Charact.*, 2016, vol. 114, pp. 254–62.

12. W. Elber, Ph.D. Thesis, University of New South Wales, Australia, 1968.
13. H. Mayer, M. Papakyriacou, B. Zettl, and S.E. Stanzl-Tschegg: *Int. J. Fatigue*, 2003, vol. 25 (3), pp. 245–56.
14. L.H. Rettberg, J.B. Jordon, M.F. Horstemeyer, and J.W. Jones: *Metall. Mater. Trans. A*, 2012, vol. 43A (7), pp. 2260–74.
15. Y. Lu, F. Taheri, M.A. Gharghouri, and H.P. Han: *J. Alloys Compd.*, 2009, vol. 470 (1–2), pp. 202–13.